Received: 18 December 2022 | Revised: 5 March 2023 | Accepted: 7 March 2023

DOI: 10.1002/jbm.a.37533

RESEARCH ARTICLE

Society For Biomaterials | WILEY

Unveiling the main factors triggering the coagulation at the SiC-blood interface

Zümray Vuslat Parlak[1] | Norina Labude-Weber[2] | Kerstin Neuhaus[3] | Christina Schmidt[3] | Aaron David Morgan[2] | Rafał Zybała[4] | Jesus Gonzalez-Julian[1] | Sabine Neuss[2,5] | Karolina Schickle[1]

[1]Department of Ceramics, Institute of Mineral Engineering, RWTH Aachen University, Aachen, Germany

[2]Institute of Pathology, RWTH Aachen University Hospital, Aachen, Germany

[3]Forschungszentrum Jülich GmbH, Institute of Energy and Climate Research, IEK-12, Helmholtz-Institute Münster: Ionics in Energy Storage, Münster, Germany

[4]Łukasiewicz Research Network, Institute of Microelectronics and Photonics, Warsaw, Poland

[5]Helmholtz Institute for Biomedical Engineering, Biointerface Group, RWTH Aachen University Hospital, Aachen, Germany

Correspondence
Zümray Vuslat Parlak, Department of Ceramics, Institute of Mineral Engineering, RWTH Aachen University, Forckenbeckstr 33, 52074 Aachen, Germany.
Email: parlak@ghi.rwth-aachen.de

Funding information
Deutsche Forschungsgemeinschaft

Abstract

Hemocompatibility is the most significant criterion for blood-contacting materials in successful *in vivo* applications. Prior to the clinical tests, *in vitro* analyses must be performed on the biomaterial surfaces in accordance with the ISO 10993-4 standards. Designing a bio-functional material requires engineering the surface structure and chemistry, which significantly influence the blood cell activity according to earlier studies. In this study, we elucidate the role of surface terminations and polymorphs of SiC single crystals in the initial stage of the contact coagulation. We present a detailed analysis of phase, roughness, surface potential, wettability, consequently, reveal their effect on cytotoxicity and hemocompatibility by employing live/dead stainings, live cell imaging, ELISA and Micro BCA protein assay. Our results showed that the surface potential and the wettability strongly depend on the crystallographic polymorph as well as the surface termination. We show, for the first time, the key role of SiC surface termination on platelet activation. This dependency is in good agreement with the results of our *in vitro* analysis and points out the prominence of cellular anisotropy. We anticipate that our experimental findings bridge the surface properties to the cellular activities, and therefore, pave the way for tailoring advanced hemocompatible surfaces.

KEYWORDS
bioceramics, cellular anisotropy, hemocompatibility, platelet activation, SiC single crystals, surface potential

1 | INTRODUCTION

Blood-contacting materials are essential elements of cardiovascular applications. Despite the advances in blood-contacting implants, hemocompatibility still must be improved in order to demonstrate their intended functionality. The implant surfaces act as foreign agents to the blood cells, triggering the coagulation cascade, independent of their types and replacement periods.[1] This effect can be overcome by systematic anticoagulant therapy, which is associated with an increased risk of bleeding. Anticoagulants are classified as high-alert medications, according to the Institute of Safe Medication Practices (ISMP).[2]

To explain the distinct behavior of blood cells on material surfaces and on purely hemocompatible endothelium, interdisciplinary research

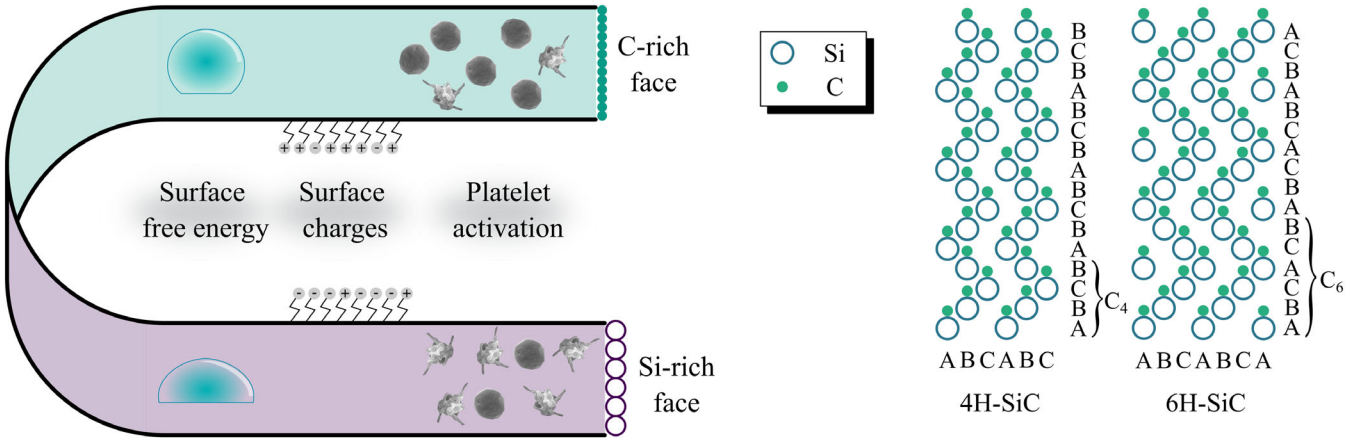

FIGURE 1 (Left) Surface properties mainly define the interactions at the material-cell interface. Depending on the surface termination Si (0001) and C (000$\bar{1}$), surface properties can reveal significant differences initiating different cell answers. (Right) The illustration of the Si-C bilayers of the 4H (ABCB) and 6H (ABCACB) hexagonal polytypes of SiC, highlighting the effect of atomic stacking on the unit cell which repeats distance along the c-axis [0001]. Both polytypes have hexagonal crystallographic structures.

must be performed including the intrinsic surface characteristics and their blood cell responses. Any neglected parameter usually results in a change in the complex cell signals. Therefore, all specific features of the material should be systematically examined prior to *in vitro* experiments.[3]

The substantial factors determining the cell-surface interaction can be listed as follows: roughness,[4,5] stiffness,[6] wettability,[7] surface charges,[8,9] and naturally, the test conditions.[10] All these factors are interconnected, leading to the complex understanding of the origin of anchorage-dependent cell behavior. On the other hand, it is assumed that the irreversible process of thrombosis is mainly triggered by interface electrochemistry when the blood cells interact with surface atoms.[11] In many conditions, charge transfer occurs in between blood components and the surface to maintain the electrochemical equilibrium, which may in turn induce the conformation of blood coagulation factors as a result of the sequential enzyme reactions.[12] This precisely regulated charge balance is suggested as a prerequisite for stable blood circulation in the body.[13–15]

Eley and Spivey investigated the electrochemistry of the blood proteins and polypeptides and showed that they have semiconducting properties with bandgap energies between 2.6 and 3.1 eV.[16] The above-mentioned charge transfer is expected to be avoided when the adjoint surface has the same semiconducting properties.[17] In that sense, SiC has been highly attractive for its semiconductive and biocompatible properties for biosensing and cardiovascular applications.[18,19] However, the understanding of surface-related effects on hemocompatibility is still not well-established.

SiC consists of sequential bilayers of silicon and carbon. Depending on the stacking sequence of the bilayers, over 200 polytypes exist.[20] The most known hexagonal forms are 4H and 6H polymorphs, which have bandgap energies of 3.2 and 3.0 eV, respectively.[21] These polymorphs are basically oriented along the direction of bilayer stacking.[22] As a consequence, a unique surface property is observed; purely terminated Si atoms in (0001) plane and purely terminated C atoms in (000$\bar{1}$) plane, see Figure 1.

In this study, we focus on SiC single crystals and their interfacial response with blood cells. With different energy gaps, polymorphic properties, and different surface terminations on (0001) and (000$\bar{1}$) crystallographic planes, 4H- and 6H- SiC crystals exhibit an ideal surface for this research. To date, the critical role of two different surface terminations of SiC (C and Si) on blood cell activation has not been reported. As a result of this work, we proved that different surface terminations of single-crystalline SiC exhibit different cell responses. Furthermore, certain surfaces inhibit the electrochemical reactions at the blood-material interface and reduce protein adsorption as well as platelet activation significantly.

2 | MATERIALS AND METHODS

Two different polymorphs, 4H and 6H, and surface terminations, C-rich and Si-rich, of single-crystalline SiC were investigated. In addition to the materials of interest, we used a chemically resistant borosilicate cover glass as a negative control and a toxic control sample treated with Triton X-100 for the cytocompatibility tests. Also, we used an endothelium monolayer as a pure hemocompatible surface control. Preparation steps of endothelial monolayer were previously described.[23]

2.1 | Preparation and microstructural characterization of SiC single crystals

High-quality silicon carbide single crystals were grown on C-faced (0001) 6H-SiC seed crystals using a physical vapor transport (PVT) technique. The growth process was carried out under argon-nitrogen (99:1) mixture atmosphere. During the first 6 h of the process, the ambient pressure was gradually reduced from 600 mbar to 50 mbar, and then kept constant for the rest of the crystal growth. The SiC source powder was heated using a graphite resistance heater up to a

crucible temperature of 2200–2300°C, while it was in the range of 2100–2200°C at the backside of the crystal. The distance between the source powder and the seed was varied from the initial distance of 50 mm down to 40 mm as the growth proceeds. These parameters yield a growth rate of 0.05–0.2 mm/h. The crystalline 4H and 6H SiC samples were cut in squares of 5 x 5 mm^2. The 1 mm thick samples were epi-polished on both sides using a diamond suspension with diamond grain size of 16, 6 and 1 µm, respectively, each for 30 min.[24] Hereafter, the samples are labeled as 4H-SiC and 6H-SiC, respectively.

2.2 | Structural and surface characterization

The polytype of SiC was determined after the XRD analysis of SiC powders. The powders were produced by grinding the single crystalline SiC substrates. The average grain diameters are 50.2 and 68.9 µm for 4H-SiC and 6H-SiC, respectively, as measured by particle size analyzer (Mastersizer 2000, Malvern PANalytical, UK). The XRD measurements were performed using an Empyrean™ 3rd Gen. diffractometer from Malvern PANalytical, featuring an ICore optical system and a GaliPIX3D area detector allowing for fast measurements. The divergence was set to 0.25° with the masks arranged to illuminate a spot of approximately 10 mm width. The powders were positioned on a zero-background-holder made of a silicon single crystal. After the analysis, crystalline phases were verified by *Highscore Plus* software. Structural data were obtained via COD and ICSD.

Surface roughness and surface potentials were measured in parallel with a Cypher ES AFM system (Oxford Instruments, UK) equipped with Pt-coated PPP-NCST-Pt tips (Nanosensors, Switzerland). The samples were measured in atmospheric conditions at a constant sample temperature of 37°C comparable to physiological thermal conditions of blood cells. The surface potential was measured using Kelvin Probe Force Microscopy (KPFM) in a dual-pass experiment. For this, the sample topography was mapped in intermittent contact mode in the first pass and the surface potential was measured during a second scan of the same line with a fixed average height difference (in our case 30 nm) between the vibrating tip and the sample surface. The mean square height (Sq) and the developed interfacial area ratio (Sdr) of a batch of topography images were calculated according to the ISO 25178 standards.

To compare the wettability of the surfaces, contact angle measurements were performed in static (Sessile drop method) and dynamic modes (tangent-2 method) with a drop shape analyzer system (DSA 100, Krüss, Germany). Prior to these experiments, the samples were first rinsed with ethanol and then with distilled water, to prevent the influence of contamination. A prescribed amount of distilled water (5 ml) was injected on the sample for static measurements, while dynamic contact angles were measured by repeatedly wetting (advancing angle) and dewetting (receding angle). The average contact angle values were calculated statistically over three droplets measured at different spots on three specimens for each system.

2.3 | Biological characterization

Biological characterization was conducted on the cryo-preserved stocks of isolated human umbilical vein endothelial cells (HUVECs), human coronary artery endothelial cells (HCAECs, PromoCell, Germany), freshly isolated human peripheral blood mononuclear cells (PBMCs) and human blood platelets. The reason behind this variety of test cells was to observe the individual response of each main blood component to foreign surfaces. According to ethical requirements, all blood samples were collected upon donors' informed consent was obtained. We ensured the donors are healthy and had not used any medication for at least 10 days prior to the experiments.

2.3.1 | Cell culture and isolation procedures

HUVECs and HCAECs seeding

Frozen HUVECs were isolated according to the process previously described[25] and approved by the local ethics committee (Proposal number: EK116/19). Endothelial cells (HUVECs and HCAECs) were thawed at room temperature to prevent thermal shock and added into an EGM-2 medium of 10 ml (BulletKit, Lonza, Germany). The resulting cell suspension was centrifuged at 200*g* for 5 min to form a cell pellet. The pellet was resuspended in an EGM-2 medium of 10 ml. The cells were seeded in T75 cell culture flasks and cultured in a humidified atmosphere. For the experiments shown in the following sections, the culture medium was removed, and the adherent cells were rinsed using 10 ml of PBS. Following this step, 3 ml of trypsin (0,05% Tyrpsin-EDTA) was added to tissue culture flasks to detach the cells. After 3 min of incubation at 37°C, 7 ml of a cell culture medium (with 2% serum) was added to stop the trypsin reaction. The cell suspension was transferred into a 50 ml Falcon tube. After centrifugation at 200*g* for 5 min, the supernatant was completely removed, and the cell pellet was resuspended in a defined volume of fresh culture medium. For the live/dead stainings, HUVECs (passages 2–3) were seeded on sterilized samples in 48-well plates with a density of 2.6×10^4 cells/cm^2 and incubated for 24 h. For live cell imaging, HCAECs (passages 3–5) were seeded on sterilized samples in 48-well plates with a density of 10×10^4 cells/cm^2, then incubated for 7 days.

Peripheral blood mononuclear cell isolation

For the PBMC isolation process, human blood was venipuncture with a Safety-Multifly needle in 6 × 7.5 ml S-Monovette Plasma Lithium-Heparin tubes and then transferred into a 50 ml Falcon tube. Three milliliters of blood were added into a 15 ml Falcon tube with an equal volume of Ficoll solution (Sigma-Aldrich, Germany), which is a hydrophilic polysaccharide to separate layers of blood. We strictly had to avoid any physical stress on the cells, which might trigger cell activation. The solution was centrifuged at 400*g* for 30 min. After this centrifugation step, the blood was separated into erythrocytes, Ficoll, PBMCs, and plasma. Isolated PBMCs (including platelets and leukocytes) were transferred into a 50 ml Falcon tube and washed three times using an EGM-2 medium, by centrifuging at 250*g* for 10 min. After washing, the PBMC pellet was resuspended with an EGM-2

culture medium for static cell culture experiments and seeded on the samples in 48-well plates. Approximately 10^6 cells/cm^2 were seeded and incubated for 4 h under the same conditions as for the HUVEC culture.

Platelet isolation

For the isolation of platelets, a gradient centrifugation method was used. Freshly venipunctured blood in 10 × 2 ml S-Monovette tubes (containing 0.106 M trisodium citrate as an anticoagulant) was transferred into a 50 ml Falcon tube and centrifuged at room temperature for 15 min at 160*g* without brake. As a result of this step, erythrocytes settled down, while the buffy coat of a thin layer of leukocytes accumulated on top of them. The platelet-rich plasma, which was deposited on this layer, was transferred into a 50 ml Falcon tube. To prevent activation of the platelets during the further processes, acid citrate dextrose (ACD) buffer was added with a volume of 10% of the collected fraction. Afterwards, centrifugation was applied at 980*g* for 5 min (without break) to obtain a platelet pellet. Platelet-poor plasma above the pellet was removed, and 18 ml of Tyrode buffer was added.

2.3.2 | Enzyme-linked immunosorbent assay

Activation and adhesion of platelets on single-crystalline ceramics were quantitatively investigated by an indirect enzyme-linked immunosorbent assay (ELISA). P-selectin, which is a released protein from activated platelets, was detected by a Purifed Mouse Anti-Human CD62P antibody. As a full activation control (positive control), platelet solution was transferred to an empty 24 well plate. This assay was performed after the dynamic flow incubation of isolated platelets on the ceramic samples. Physiological blood flow condition of human coronary artery was simulated using a bioreactor system (MinuCell and MinuTissue perfusion chamber systems, Munich). A laminar flow (100 ml\min) of the platelet solution over the samples was generated for 30 min at 37°C. After the incubation time, antibodies were coupled, and the samples were transferred to a new microtiter plate. By this way, the enzymatic conversion by the antibody-bound horseradish peroxidase is achieved only through antibodies bound to the sample surfaces. Subsequently, the intensity of UV-marker was measured using Tecan microplate reader at 450 nm. Detailed steps of the ELISA were described previously.[26]

2.3.3 | Micro BCA protein assay

All sample surfaces were incubated in the platelet-poor plasma (PPP, 300 µl/cm^2) for 30 min at 37°C. The isolation procedure of PPP was previously described in the *Cell culture and isolation procedure* section. After the incubation, the surfaces were washed with PBS. Adsorbed protein concentrations on the sample surfaces were quantified using a Micro BCA Protein Assay Kit (ThermoFisher Scientific), according to the manufacturer´s instructions. The light absorbance of the protein solutions was measured by a Tecan microplate reader at 562 nm. The protein concentration values were analyzed based on the standard curve plotted for each sample.

2.3.4 | Live/dead staining

Propidium iodide (PI; Sigma, Steinheim, Germany) and fluorescein diacetate (FDA; Sigma, Steinheim, Germany) were used for performing live/dead staining according to the ISO 10993-5 standards. 10 µl of PI (0.5 µg in PBS) and 10 µl of FDA (5 µg/ml in acetone) were added into 600 µl of Ringer solution (Delta-Pharma, Pfullingen, Germany) to create the staining solution. Then, 20 µl of the staining solution was added to the seeded specimens and imaged using a fluorescence microscope (Axio imager, Zeiss, Germany). Live and dead cells were distinguished according to their fluorescent colors (green and red, respectively) and quantified using the ImageJ software.

2.3.5 | Cellcyte X live cell imaging

A Cellcyte X (Cytena, Germany) live cell imaging system was used to monitor the viability and proliferation of cells on material samples. In preparation for imaging with this system, all cells were stained using 20 µl of Celltracker Green CMFDA Dye (Thermofischer, Germany) per 10 ml of culture medium and incubated at 37°C for 15 min. The SiC samples were then moved to a new well plate with 2 ml of fresh culture medium to exclude any cells that were not adhered to sample surfaces. The well plate containing the cellularized materials was then placed into the Cellcyte X. Each well was imaged using nine adjacent, nonoverlapping fields of view arranged in 3 x 3 grid. The fields of view containing the cellularized material were chosen for analysis. Imaging in the green fluorescent channel used an exposure time of 150 ms and a gain of 2 dB. Each field of view was imaged once every 3 h over a period of 7 days in both the "enhanced countour" (brightfield analog) and green fluorescent channel. Cell culture medium was exchanged every 48 h, without interrupting imaging. Subsequently, confluency analysis was performed using Cellcyte Studio (Cytena, Germany) on the fields of view containing cellularized material. The surface area of the material covered by the endothelial cells was measured and exported for comparison.

2.3.6 | Scanning electron microscopy analysis

Scanning electron microscopy (SEM, Philips XL 30, Field Emission Gun) was used to image the morphology of the cells and their adherence and activation at SiC single crystals and control materials. In order to prepare the samples for SEM, incubated cells were fixed with 3% glutaraldehyde without previous washing steps and then stored at 4°C. Prior to SEM imaging, the samples were dehydrated with ethanol 70% and dried with hexamethyldisilazane. The dried samples were coated with gold–palladium and scanned using secondary electrons.

2.4 | Statistical analysis

All experimental values are represented as mean ± SD. Statistical significance was evaluated by One-way ANOVA with Tukey´s multiple comparison test using GraphPad Prism version 9.0.0 for Windows, GraphPad Software, San Diego, California, USA. A value of $p < .05$ was considered statistically significant.

TABLE 1 Surface roughness of single crystalline samples measured by atomic force microscopy (AFM). The mean square height of an image (Sq) is calculated over an area of 100 μm^2. The developed interfacial area ratio (Sdr) is given in the second row which basically indicates the complexity of the surface.

	4H-SiC-C	4H-SiC-Si	6H-SiC-C	6H-SiC-Si
Sq (nm)	7.89 ± 5.41	2.98 ± 0.08	5.33 ± 1.64	2.21 ± 0.10
Sdr (%)	0.73 ± 0.55	1.48 ± 0.06	0.57 ± 0.24	0.10 ± 0.05

3 | RESULTS

3.1 | Intrinsic surface characterization

Polymorphs of the silicon carbide single crystals were confirmed prior to further surface characterization. Two polytypes of SiC (4H and 6H) were identified by the main peaks observed in the x-ray diffraction patterns, which precisely matched with the ICSD reference data, as shown in supplementary. The 4H-SiC polymorph exhibits the well-defined

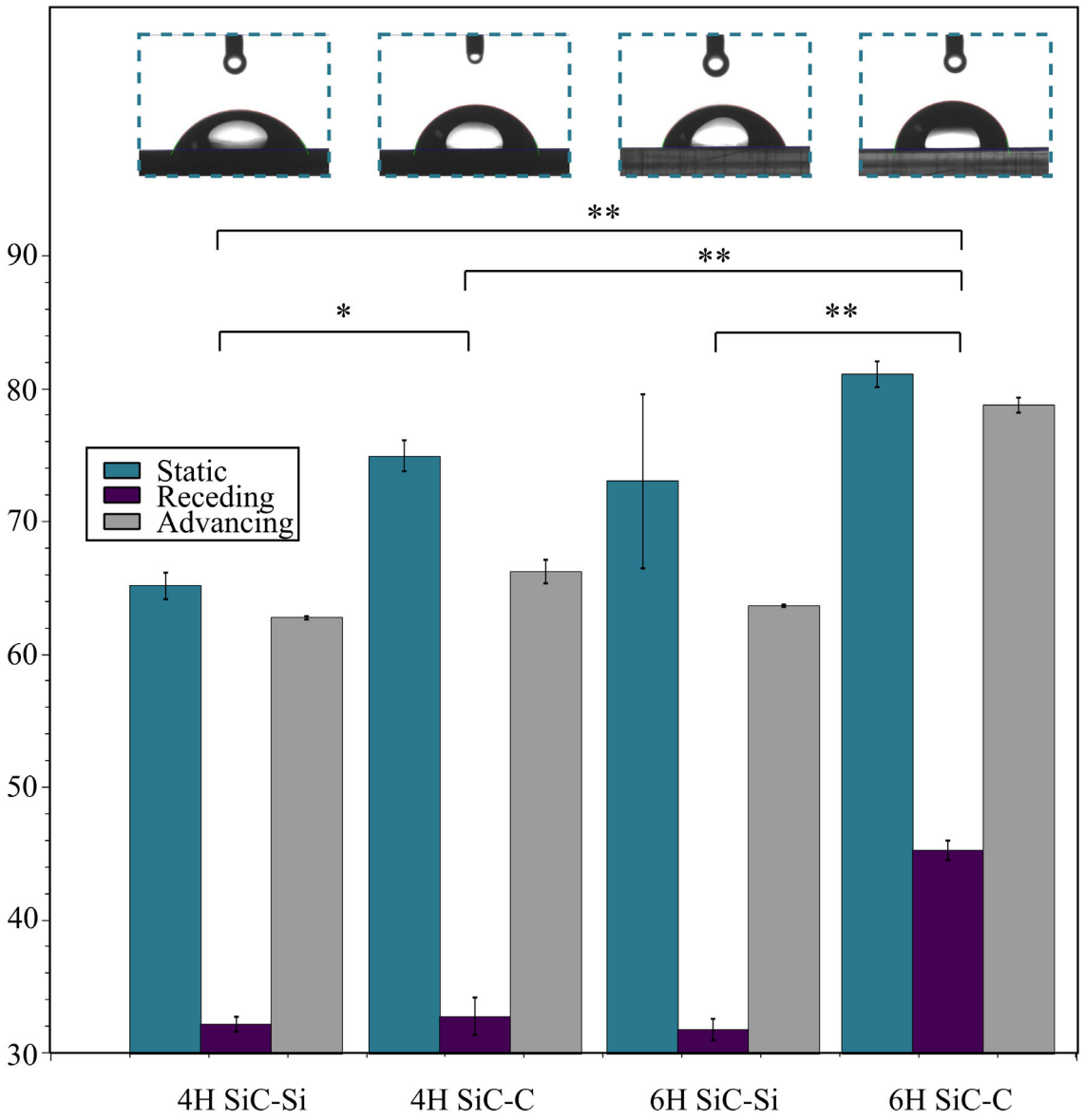

FIGURE 2 Static, receding and advancing contact angles and water drop profiles for various SiC single crystals. Error bars show the standard deviations for 3 measurements at each of the 3 regions of interest on the samples, *$p < .008$, **$p < .0001$.

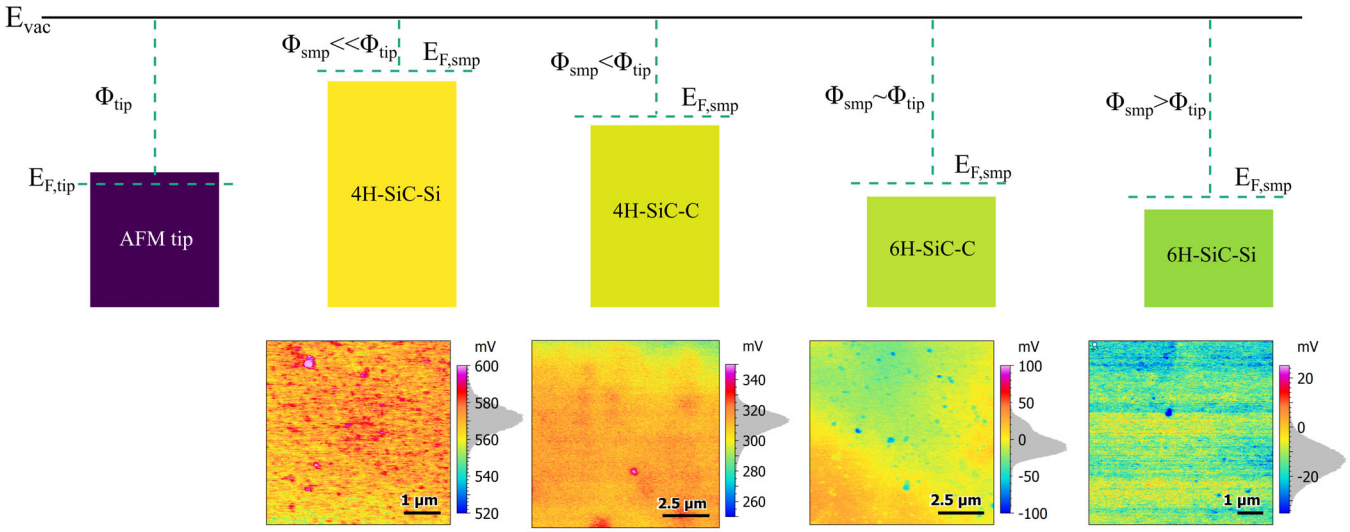

FIGURE 3 Schematized picture of the Fermi energy levels and work functions of the crystals and the AFM tip after the contact and charge transfer. Corresponding exemplary surface potential maps measured using KPFM are given below.

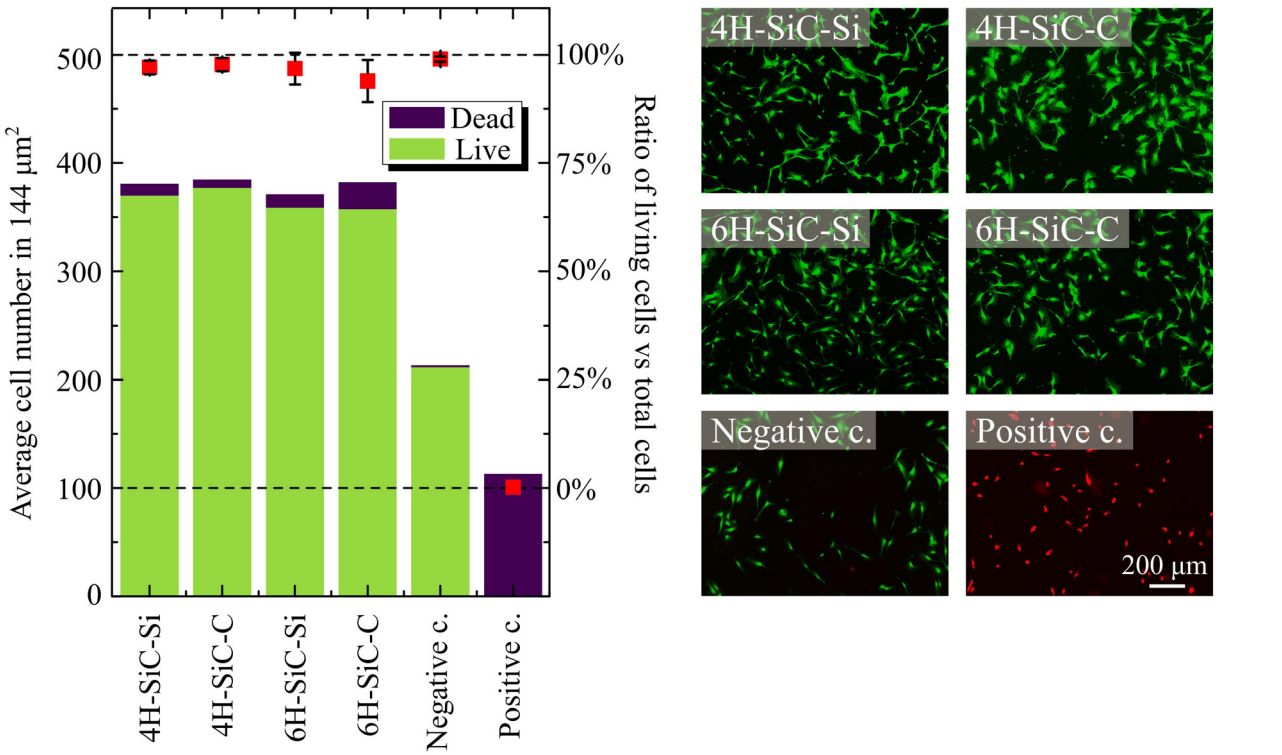

FIGURE 4 (Left) Average numbers of viable and dead HUVECs on single crystals and controls after 24 h incubation. Calculated dead-live cell ratios are shown in the right ordinate and depicted with white squares. (Right) Live/dead stainings of single crystals and control materials under fluorescence microscopy. The size of the error bars reflects $n = 3$ repetitions. The built-in tools of ImageJ image analysis software were used to count the cells, and 2 images were evaluated per donor.

identical peaks at 43.3° and 49.8°. On the other hand, 6H-SiC was clearly distinguished from the 4H polymorph by its identical peaks at 34.1° and 45.3°.

Surface roughness was characterized using AFM. Sample surfaces exhibit a comparable average roughness, ranging between 2.21–7.89 nm, see Table 1. C-faces of both 4H and 6H polymorphs showed slightly larger surface roughness than those of Si-faces. Considering the size of the platelets (~2 µm), the difference in surface roughness (~5 nm) was neglected and assumed to create equal shear stress levels over the cells.

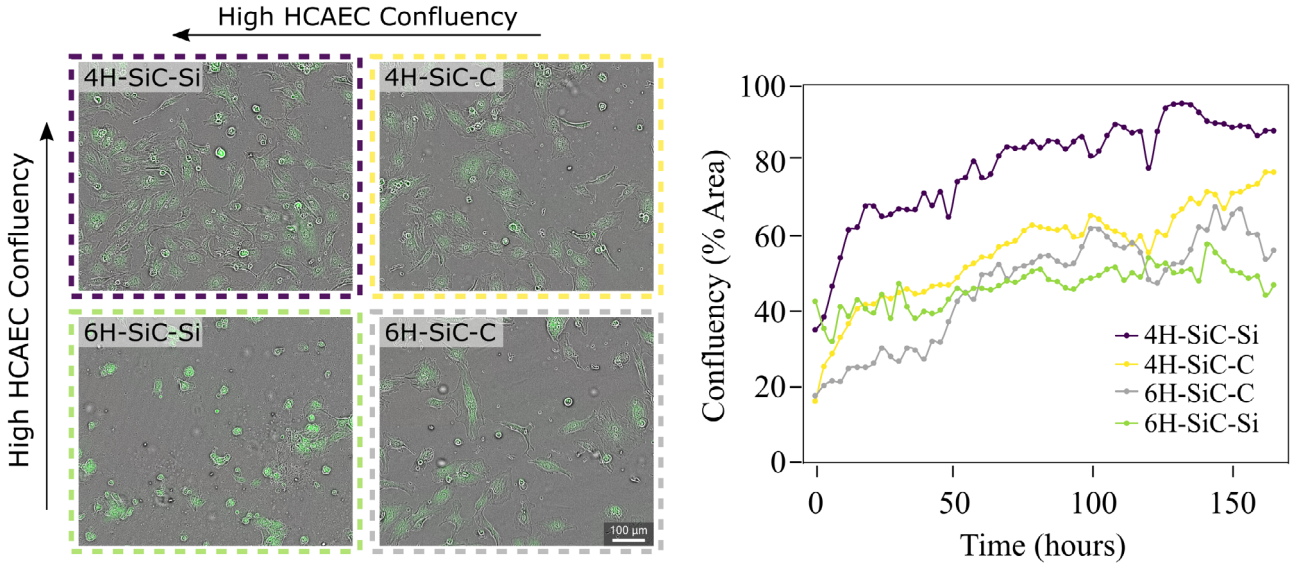

FIGURE 5 (Left) Live cell images of HCAECs after 30 h of incubation period. (Right) Cell confluency graph measured by Cellcyte X live imaging over 7 days incubation period of HCAECs on different surfaces. The confluency graph was calculated for one exemplary donor and represents 9 regions of interest over the samples.

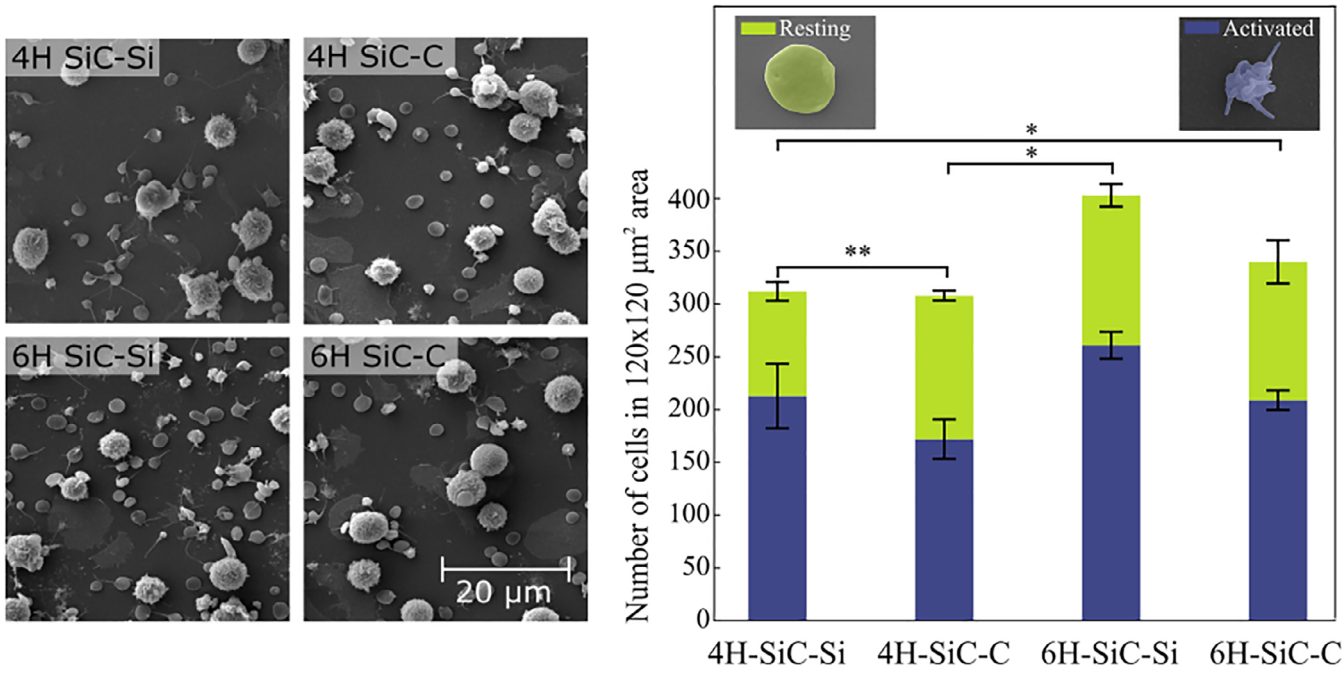

FIGURE 6 (Left) SEM images of isolated PMBCs in four different surfaces. The images include platelets (discoid shapes, ~2 µm in diameter) and leukocytes (round shapes with distinct membranes, ~10 µm in diameter) as well. (Right) The graph indicates the number of activated and resting platelets after 4 h incubation on the SiC polytypes under static conditions. Each within 120 x 120 µm^2 area of interest. Resting platelets are depicted in green and activated platelets are depicted in blue color. Standard deviations on the graph are calculated from one representative experiment over 3 SEM images per system ($n = 3$, $^*p < .02$, $^{**}p = 0.0008$).

Regarding the wettability, the measured contact angles confirm that all samples are of hydrophilic nature, which differs only in the magnitude (Figure 2). The magnitudes of the C- and Si-faces of SiC were significantly different for both SiC polymorphs. The results were correlated with each other and verified that Si-faces exhibit higher wettability than C-faces while for the same type of faces 4H polytype show higher wettability.

The surface potential of 4H-SiC-Si is measured to be in the range of 500–580 mV, which is approximately 200 mV larger than that of 4H-SiC-C, which is in the range of 300–350 mV (Figure 3).

Both faces of the 4H polymorph show considerably larger surface potentials than the surfaces of 6H polymorphs. The surface potentials of 6H-SiC-C samples are in the −20 to 20 mV range, which is several hundred mV lower and also narrower than the range of the 4H samples.

3.2 | Cytocompatibility

The amount of viable and dead cells on different surfaces were analyzed with the live/dead staining assay. Based on the findings, all single crystalline specimens were verified to be cytocompatible with HUVECs and blood cells. They demonstrated high viability rates indicated by green fluorescence (Figure 4, right). As typical for the positive control, cells showed strong red fluorescence by virtue of completely permeabilized membranes. This means the cells on the positive control are 100% dead due to the intense toxicity of the chemically treated environment. The lowest number of viable adherent cells was found on the negative control samples (glass) which point out that the adhesion rate of the HUVECs on the SiC surface is higher than on the negative controls, (Figure 4, left). There was no difference regarding the viability rates of 4H-SiC and 6H-SiC and their different faces C and Si.

3.3 | The HCAECs confluency

A clear difference was observed between the SiC polymorphs (Figure 5). When comparing confluency (% area covered by cells), both surface terminations of 4H-SiC showed higher confluency than the 6H-SiC surfaces. The largest difference was seen when comparing 4H-SiC-Si to the other conditions. The 4H-SiC-Si showed greatly increased confluency and maintained this increased confluency throughout the experiment. Endothelial cells on 4H-SiC-Si became nearly completely confluent (96%), while the other materials showed much lower maximum confluency (4H-SiC-C: 78%, 6H-SiC-C: 68%, 6H-SiC-Si: 58%). It was also observed that the rate of increase in confluency over the course of the study was similar among all materials, except during the first 24-h period. During this period, cells on 4H-SiC-Si showed a greatly increased rate of confluency, when compared to the other surfaces.

3.4 | Platelet activation and protein adsorption

Platelets were examined for their degree of activation quantitatively and qualitatively by SEM and ELISA. The platelets were evaluated according to their morphologies as discoids, pseudopodial, dendritic and fully spread. Platelets showing circular morphology without extending pseudopodia, were counted as resting state while the remaining morphologies were counted as activated. Leukocytes were excluded from the calculations. The graph in Figure 6 provides the statistical number of activated platelets on the specimens. Our results clearly indicated the increase in platelet activation on the Si face for both 4H and 6H polytypes. The activated cells were characterized by the reversal of their discoid shape and the released pseudopods. The ratio of activated platelets was 10.3% (4H) and 12% (6H) higher on Si-faces than on C-faces. In addition, we observed a slightly higher number of adhered cells on the 6H-SiC, which is consistent with the detected P-selectin levels by ELISA (Figure 8, right).

To get a clearer insight into the relationship between cell activation, surface wetting, and surface potential, we summarize the respective results in Figure 7. The highest platelet activation was observed on the 4H-Si surface, which also exhibits the highest surface potential and wettability (the lowest contact angle) as well. Platelet activations and wettability are higher on the Si-terminated surfaces in both 4H and 6H.

Both 4H and 6H polytypes of SiC samples exhibited low absorption of CD62P marker for activated platelets when compared to the positive control (Figure 8, right). Platelet solution in 24 well plate without sample material was used as a positive control while pure Tyrode

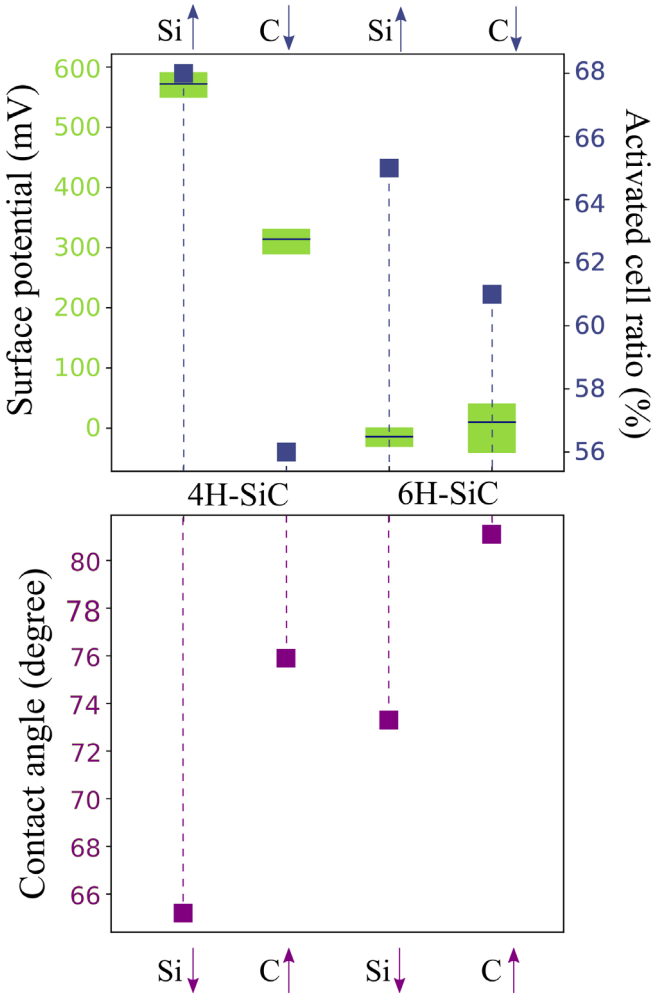

FIGURE 7 Above: Platelet activation dependence on the surface potential. Measured surface potentials are depicted by green bars while the black line represents the central potential value. The activated cell ratios are depicted by blueish squares. Below: Average contact angle values for the identical samples.

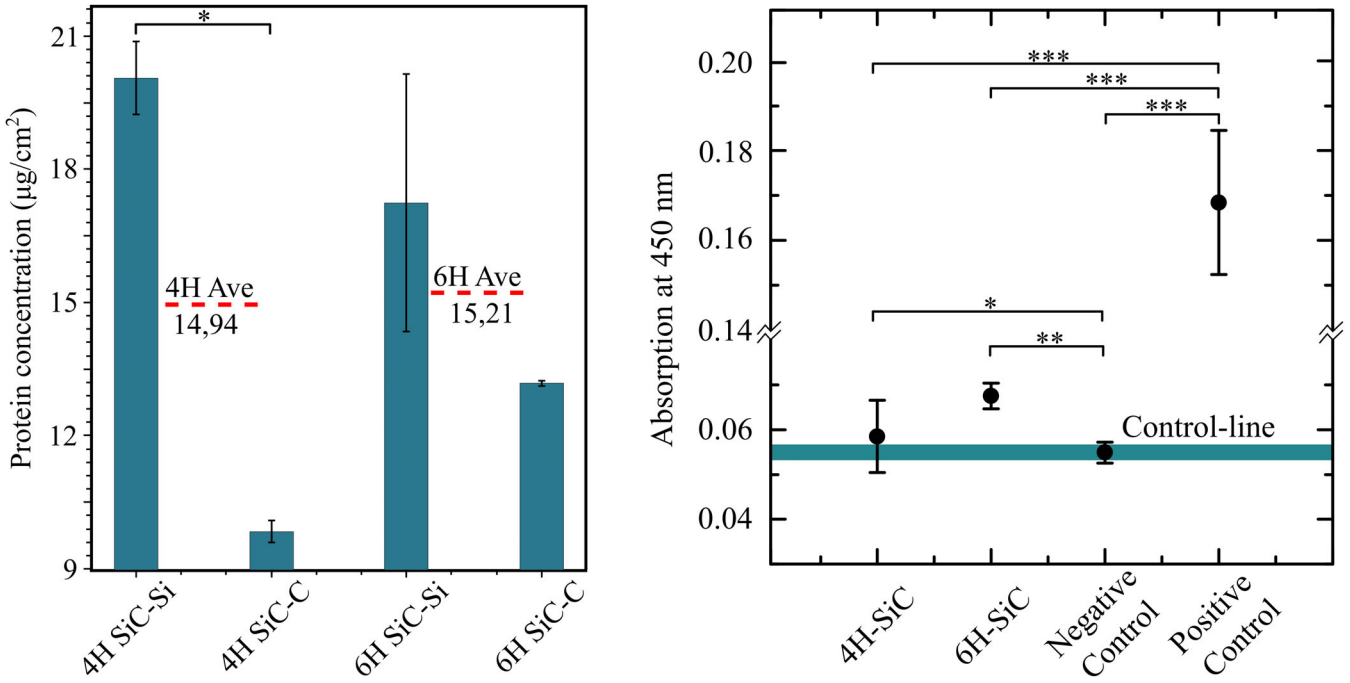

FIGURE 8 (Left) Adsorbed proteins measured by Micro BCA protein adsorption kit. Average adsorbed protein concentrations on the 4H and 6H polymorphs are depicted in red ($n = 2$, $^{*}p < .03$). (Right) The results of the ELISA in terms of absorption of CD62P activated platelets marker at 450 nm wavelength ($n = 3$, $^{*}p < .05$, $^{**}p < .005$, $^{***}p < .0001$).

buffer without platelets was used as a negative control. The UV absorption of 4H-SiC is slightly above the control line where both polytypes 4H and 6H are significantly lower than the full activation level of the positive control. It is significant that the average CD62P exposure of 4H SiC is lower than 6H-SiC which indicates lower platelet activation.

Adsorbed proteins on the sample surfaces were quantified using Micro BCA Protein Assay. Figure 8 shows the adsorption profile of the blood plasma proteins. The average concentration of protein adsorption on 4H-SiC is 14,94 µg/cm^2, while on 6H-SiC is 15,21 µg/cm^2. On the other hand, the Si-terminated faces have significantly larger protein concentrations than the C-terminated faces. The rate of increase is estimated as 104% for 4H polymorph and 31% for 6H polymorph.

4 | DISCUSSION

We performed a comprehensive study on the semiconducting SiC single crystals to reveal the specific surficial factors affecting hemocompatibility. Earlier reports showed that platelet activation can be inhibited if the surface is a semiconductor like blood proteins.[16] Therefore, it is reasonable to expect to maintain the electrochemical equilibrium at the semiconductor-blood interface employing SiC surfaces. Furthermore, SiC allows for investigating two surfaces purely terminated by either Si or C atoms to compare surface parameters on platelet activation (Figure 1). The presence of its 4H and 6H polymorphs is a good comparison of the surfaces regarding their different band gap energies and surface potentials. Owing to the fact that these hexagonal polymorphs were grown on the same seed under the same conditions, we could also eliminate the side effects and use crystallographic polymorph as a control parameter.

The 4H and 6H polymorphs of SiC showed lower hemocompatibility levels compared to previously examined surfaces, e.g., alumina ($11\bar{2}0$).[23] In the case of cytocompatibility, HUVECs on two SiC polymorphs did not exhibit a notable difference in the viability rates (Figure 4). These findings are in a very good agreement with Coletti et al.[27] We also verified the similar thrombogenic characteristics, i.e., the average number of activated platelets, adsorbed protein concentration and surface-expressed P-selectin levels of 4H and 6H (Figure 6 and Figure 8), besides the slight differences, correlated with the findings of Schettini et al.[28] The reason for the similar values between two polymorphs of SiC may be attributed to the same surface termination of (0001) plane (Si-rich) and ($000\bar{1}$) plane (C-rich). Even if the stacking orders of the atoms are different, both polymorphs are oriented along the c-axis, and possess the same surface terminations during the contact activation.

Although the polymorphs affect the cell behaviors in a similar trend, the difference in the stacking number of the atoms, 4 for 4H-SiC and 6 for 6H-SiC gave a rise to variation in surface potentials (Figure 3). This originates from the differences in the band gap energy with the change in the number of bilayers in hexagonal SiC.[18] In the case of intrinsic (undoped) semiconductors, the Fermi level is around the middle of the band gap.[29] By measuring the work function differences with KPFM, we estimated the positions of Fermi levels of each sample relative to each other (Figure 3). In the literature, 4H-SiC has the highest bandgap (Eg = 3.2 eV) among the other polymorphs of SiC.[18] Consistent with the results in the literature, the surface

potential and the position of the Fermi level of 4H-SiC were higher than the 6H-SiC in our measurements (Figure 3). Considering the effect of this difference on the blood cell behavior, the highest activation rates of the platelets and protein adsorption are observed at the highest potential level (Figure 7). However, the role of surface potential on blood cell activation has not been conclusively proven by our findings, because the difference in cell activations is diminutive for 4H- and 6H- SiC (Figure 6). The large difference between the surface potentials of 4H and 6H is not projected on the cell activation (Figure 7). Here, the factors severely distort the measurements during the surface potential analysis have to be mentioned. Measurements were conducted under dry conditions, which inhibits the simulation of the physiological conditions. The adsorbed species on the sample and the tip decreases the accuracy of the data. On the other hand, KPFM measurements in a dry state present the most feasible method to obtain a quantitative comparison of Fermi levels, which is the underlying effect in cell behaviors. Supporting this, HCAECs showed significant correlation between surface potential and cell confluency (Figure 5). Previously, it has been reported by Kao et al. that fibroblast cells on high-potential surfaces undergo less repulsion, and thus, their adsorption rates to the surface appear to be faster than the ones with lower surface potential.[30] We have also demonstrated that the 4H-SiC surfaces show greater endothelial cell confluency across the entire 7-days observation period, with 4H-SiC-Si showing near complete confluency and achieved this confluency at a much higher rate than the other surfaces.

Besides the polymorphs, surface terminations, i.e., crystallographic planes have a deeper effect on blood cell behaviors. The lower platelet activation levels on the C-rich face indicate a better hemocompatible behavior than on the Si-rich face. Figure 6 clearly indicates that Si-terminated surfaces are more prone to platelet activation than C-terminated surfaces, which correlates to the contact angle values. This is a consequence of different electronegativities of C (2.55, Pauling scale) and Si (1.9, Pauling scale) determining the adsorption of hydroxyl (-OH) and carboxyl (-COOH) groups.[31] Therefore, stronger bonds will be created between hydroxyl groups and the Si-rich face, which also explains the higher wetting on the Si-rich face. We note that the terminated surfaces with functional groups are more likely adhered by Mammalian cells.[32] This explains our findings on the increased platelet activation (Figure 6) and initial endothelial cell adhesion on the Si-rich face (Figure 5). In relation to this, Cai et al. showed that adsorbed oxygen content of the functional groups increases the polar component of surface free energy, resulting in the wetting of the surface and enhancing the cell adhesion indirectly via blood proteins such as vitronectin and fibronectin adsorption.[33]

Blood proteins play a decisive role in surface-induced thrombosis. When the material interacts with blood, plasma proteins are adsorbed to the surface immediately upon contact and form a layer mediating the platelet adhesion via cell membrane receptors.[11] We compared the total amount of the adsorbed proteins on different polymorphs and terminations of SiC (Figure 8, left). Adsorbed proteins at the Si-rich face were considerably higher than the C-rich faces for both polymorphs, consistent with higher platelet activations. For further exploration of the correlation between protein adsorption and contact activation has to be investigated in three complement aspects: the quantity of adsorbed proteins, the composition of the adsorbed protein layer, and the conformation of the adsorbed proteins.[34–36]

5 | CONCLUSION

Our study revealed that two surface terminations of SiC (Si-rich (0001) and C-rich ($000\bar{1}$)), of which the role in most of the hemocompatibility experiments has so far been neglected, can lead to significant differences in terms of platelet activation. We have also clearly shown the effect of crystallographic polymorph (4H and 6H) in high endothelial cell confluency, directly related to surface potential. From this critical difference, we are now one more step closer to understanding the overall blood activation mechanism, highlighting the critical importance of crystallographic plane and polymorph on the cellular behaviors.

ACKNOWLEDGMENTS

The authors thank Ms. Chloé Radermacher for her support for the blood collection, and Mr Philipp Jacobs for the XRD measurements. All blood donors are highly appreciated. This research was funded by Deutsche Forschungsgemeinschaft (DFG, German Research Foundation) - 405895710. Open Access funding enabled and organized by Projekt DEAL.

DATA AVAILABILITY STATEMENT

The data that support the findings of this study are available from the corresponding author upon reasonable request.

ORCID

Zümray Vuslat Parlak https://orcid.org/0000-0003-0691-9184

REFERENCES

1. Jaffer IH, Jeffrey IW. The blood compatibility challenge. Part 1: blood-contacting medical devices: the scope of the problem. *Acta Biomater*. 2019;94:2-10.
2. Amaraneni A, Chippa V, Rettew AC. Anticoagulation safety. May 24, 2022. In: StatPearls. treasure island (FL): StatPearls publishing; 2022 Jan. PMID: 30085567.
3. Rahmati M, Silva EA, Reseland JE, Heyward CA, Haugen HJ. Biological responses to physicochemical properties of biomaterial surface. *Chem Soc Rev*. 2020;49(15):5178-5224.
4. Linneweber J, Dohmen PM, Kerzscher U, Affeld K, Nose Y, Konertz W. The effect of surface roughness on activation of the coagulation system and platelet adhesion in rotary blood pumps. *Artif Organs*. 2007;31(5):345-351.
5. Tsai W-B, Grunkmeier JM, McFarland CD, Horbett TA. Platelet adhesion to polystyrene-based surfaces preadsorbed with plasmas selectively depleted in fibrinogen, fibronectin, vitronectin, or von Willebrand's factor. *J Biomed Mater Res*. 2002;60(3):348-359.
6. Vining KH, Mooney DJ. Mechanical forces direct stem cell behaviour in development and regeneration. *Nat Rev Mol Cell Biol*. 2017;18(12):728-742.
7. Xu L-C, Siedlecki CA. Effects of surface wettability and contact time on protein adhesion to biomaterial surfaces. *Biomaterials*. 2007;28(22):3273-3283.

8. Chen X, Wang J, Paszti Z, et al. Ordered adsorption of coagulation factor XII on negatively charged polymer surfaces probed by sum frequency generation vibrational spectroscopy. *Anal Bioanal Chem*. 2007;388(1):65-72.
9. Yan Y, Xu L-C, Vogler EA, Siedlecki CA. Contact activation by the intrinsic pathway of blood plasma coagulation. In: Siedlecki CA, ed. *Hemocompatibility of Biomaterials for Clinical Applications*. Woodhead Publishing; 2018:3-28.
10. Sperling C, Maitz MF, Werner C. Test methods for hemocompatibility of biomaterials. In: Siedlecki CA, ed. *Hemocompatibility of Biomaterials for Clinical Applications*. Woodhead Publishing; 2018:77-104.
11. Xu L-C, Bauer JW, Siedlecki CA. Proteins, platelets, and blood coagulation at biomaterial interfaces. *Colloids Surf B Biointerfaces*. 2014; 124:49-68.
12. Vogler EA, Siedlecki CA. Contact activation of blood-plasma coagulation. *Biomaterials*. 2009;30(10):1857-1869.
13. Rzany A, Schaldach M. Physical properties of antithrombogenic materials–an electronic model of contact activation. *Progress Biomed Res*. 1999;4:59-70.
14. Wan G, Lv B, Jin G, Maitz MF, Zhou J, Huang N. Direct correlation of electrochemical behaviors with anti-thrombogenicity of semiconducting titanium oxide films. *J Biomater Appl*. 2014;28(5): 719-728.
15. Huang, N., Yang, P., Leng, Y. X., Chen, J. Y., Sun, H., Wang, J., Wang, G. J., Ding, P. D., Xi, T. F., Leng, Y., "Hemocompatibility of titanium oxide films" 24.13 (2003):2177–2187
16. Eley DD, Spivey DI. The semiconductivity of organic substances. Part 6. A range of proteins. *Trans Faraday Soc*. 1960;56:1432-1442.
17. Hansi C, Arab A, Rzany A, Ahrens I, Bode C, Hehrlein C. Differences of platelet adhesion and thrombus activation on amorphous silicon carbide, magnesium alloy, stainless steel, and cobalt chromium stent surfaces. *Catheher Cardiovasc Interv*. 2009;73(4):488-496.
18. Saddow SE. Silicon carbide materials for biomedical applications. In: Saddow SE, ed. *Silicon Carbide Biotechnology (Second Edition)*. Elsevier; 2016:1-25.
19. Kotzar G, Freas M, Abel P, et al. Evaluation of MEMS materials of construction for implantable medical devices. *Biomaterials*. 2002; 23(13):2737-2750.
20. Fisher GR, Barnes P. Towards a unified view of polytypism in silicon carbide. *Philos Mag B*. 1990;61(2):217-236.
21. Casady JB, Johnson RW. Status of silicon carbide (SiC) as a wide-bandgap semiconductor for high-temperature applications: a review. *Solid-State Electron*. 1996;39(10):1409-1422.
22. Schoell, S. J., Oliveros, A., Steenackers, M., Saddow, S. E., Sharp, I. D. "Multifunctional SiC surfaces: From passivation to biofunctionalization. In: Saddow, S. E. (Ed.), silicon carbide biotechnology (2012): 63–117.
23. Parlak ZV, Labude N, Rütten S, et al. Toward innovative Hemocompatible surfaces: crystallographic plane impact on platelet activation. *ACS Biomater Sci Eng*. 2020;6(12):6726-6736.
24. Tymicki E, Grasza K, Diduszko R, Bozek R, Gala M. Initial stages of SiC crystal growth by PVT method. *Cryst Res Technol: J Exp Indus Crystal*. 2007;42(12):1232-1236.
25. Bienert M, Hoss M, Bartneck M, et al. Growth factor-functionalized silk membranes support wound healing in vitro. *Biomed Mater*. 2017; 12(4):045023.
26. Parlak ZV, Wein S, Zybala R, et al. High-strength ceramics as innovative candidates for cardiovascular implants. *J Biomater Appl*. 2019; 34(4):585-596.
27. Coletti, C., Jaroszeski, M. J., Hoff, A. M., Saddow, S. E. "SiC in vitro biocompatibility: Epidermal and connective tissue cells. In: Saddow, S. E. (Ed.), silicon carbide biotechnology (2012): 119–151.
28. Schettini, N., Jaroszeski, M. J., West, L., Saddow, S. E. "Hemocompatibility assessment of 3C-SiC for cardiovascular applications. In: Saddow, S. E. (Ed.), silicon carbide biotechnology (2012): 153–208.
29. Kittel C. *Introduction to Solid State Physics*. Eight ed. Wiley; 2016.
30. Kao W-L, Chang H-Y, Lin K-Y, Lee Y-W, Shyue J-J. Effect of surface potential on the adhesion behavior of NIH3T3 cells revealed by quartz crystal microbalance with dissipation monitoring (QCM-D). *J Phys Chem C*. 2017;121(1):533-541.
31. Allen LC. Electronegativity is the average one-electron energy of the valence-shell electrons in ground-state free atoms. *J Am Chem Soc*. 1989;111(25):9003-9014.
32. Curtis ASG, Forrester JV, Clark P. Substrate hydroxylation and cell adhesion. *J Cell Sci*. 1986;86(1):9-24.
33. Cai S, Wu C, Yang W, Liang W, Yu H, Liu L. Recent advance in surface modification for regulating cell adhesion and behaviors. *Nanotechnol Rev*. 2020;9(1):971-989.
34. Mei Y, Saha K, Bogatyrev SR, et al. Combinatorial development of biomaterials for clonal growth of human pluripotent stem cells. *Nat Mater*. 2010;9(9):768-778.
35. Milleret V, Buzzi S, Gehrig P, et al. Protein adsorption steers blood contact activation on engineered cobalt chromium alloy oxide layers. *Acta Biomater*. 2015;24:343-351.
36. Sivaraman B, Latour RA. The relationship between platelet adhesion on surfaces and the structure versus the amount of adsorbed fibrinogen. *Biomaterials*. 2010;31(5):832-839.

SUPPORTING INFORMATION

Additional supporting information can be found online in the Supporting Information section at the end of this article.

How to cite this article: Parlak ZV, Labude-Weber N, Neuhaus K, et al. Unveiling the main factors triggering the coagulation at the SiC-blood interface. *J Biomed Mater Res*. 2023;111(9):1322-1332. doi:10.1002/jbm.a.37533